Insight into the dehydration behaviour of scandium-substituted barium titanate perovskites via simultaneous in situ neutron powder

Solid State Ionics 324 (2018) 233–240

Contents lists available at ScienceDirect

Solid State Ionics

journal homepage: www.elsevier.com/locate/ssi

Insight into the dehydration behaviour of scandium-substituted barium titanate perovskites *via* simultaneous *in situ* neutron powder thermodiffractometry and thermogravimetric analysis

Nico Torino[a,*], Paul F. Henry[a,b], Christopher S. Knee[a,c], Samantha K. Callear[b], Ronald I. Smith[b], Seikh M.H. Rahman[a], Sten G. Eriksson[a]

[a] Department of Chemistry and Chemical Engineering, Chalmers University of Technology, SE-412 96 Gothenburg, Sweden
[b] ISIS Pulsed Neutron and Muon Source, Rutherford Appleton Laboratory, Didcot OX11 0QX, UK
[c] Now ESAB AB, Lindholmsallén 9, Box 8004, SE-402 77 Gothenburg, Sweden

ARTICLE INFO

Keywords:
Neutron powder diffraction
Thermogravimetry
In situ
Dehydration
Proton conductor
Perovskite

ABSTRACT

Hydration-dehydration cycles are critical to the mechanical performance of ceramic proton conductors. The development of *in situ* methods is desirable in order to study their structural response under conditions that mimic the operating ones. Neutron powder diffraction studies combined with simultaneous thermogravimetric analysis were performed on the hydrated forms of two members of the oxygen deficient perovskite $BaTi_{1-x}Sc_xO_{3-\delta}$ series, with $x = 0.5$ and $x = 0.7$. Rietveld analyses agreed with *in situ* gravimetric data, allowing correlation of occupancy factors of the oxygen site to hydration levels and other structural data. Dehydration is an activated process that impacts on structural parameters and the level of Sc substitution was found to control the structural response during *in situ* dehydration, with higher Sc content leading to significantly greater volume contraction. This was rationalised by the chemical expansion due to hydration of oxygen vacancies within the $x = 0.5$ sample being anomalously small. Furthermore, the behaviour of the $x = 0.5$ system revealed an unexpected cell expansion during the early stages of dehydration, suggesting the hydration level may influence the thermal expansion coefficient (TEC).

1. Introduction

The success of proton conducting-solid oxide fuel cells (PC-SOFC, or PCFC) technology relies on understanding the transport properties and probing the stability of the materials utilised to fabricate the cell. To this end, the toolkit available to the materials scientist is ever increasing, with a number of characterisation methods contributing to elucidating structure-property relationships [1]. Often, independent or *ex situ* studies fail to comprehensively explain processes, due to difficulties to exactly reproduce conditions. Hence, the development of *in situ*, *in operando* and combined method approaches is very desirable [2], and demonstrated, for example, by studies on hydrogen storage materials [3], Li-ion batteries [4], oxide systems for carbon sequestration [5], catalytic systems [6], and protonic conductors [7, 8].

High temperature proton conducting electrolytes are the benchmark among acceptor doped perovskite-type materials, with the $BaCeO_3$ and $BaZrO_3$ related phases considered as the most promising [1]; among those, Y-doped $BaZrO_3$ [9] proton conductors display the highest bulk proton conductivity [10, 11]. Commercialisation of this class of ceramic materials remains an ongoing endeavour, mainly because of the high grain boundary resistance due to a bimodal size distribution of grains [12, 13] that affects their sinterability and stability under operating conditions. Optimisation of the parameters governing densification and stability of such phases is being addressed by novel fabrication methods [14–16] and grain surface processing prior to utilisation [17].

In order to conduct protons, these oxides undergo a hydration step, illustrated in the Kröger-Vink notation by the equilibrium:

$$H_2O\,(g) + v_O^{\bullet\bullet} + O_O^{\times} \rightleftarrows 2\,OH_o^{\bullet} \quad (1)$$

where water from the gas phase is incorporated into the vacancies generated by acceptor doping the host phase, *i.e.* the original mixed oxide itself, thus creating protonic defects within the lattice in the form of hydroxyl anions at an oxygen lattice site. Hydration is usually associated with an expansion of the crystal lattice [18, 19], a phenomenon that is critical to the mechanical stability and, therefore, to the lifetime of any device, potentially leading to micro-fissures in the

* Corresponding author.
E-mail address: torino@chalmers.se (N. Torino).

https://doi.org/10.1016/j.ssi.2018.07.010
Received 5 May 2018; Received in revised form 5 July 2018; Accepted 8 July 2018
Available online 19 July 2018

electrolyte and/or delamination at the electrolyte/electrode interface. Further, filling the vacancies in systems with high levels of oxygen vacancies can produce structural phase transitions, as in the case of the orthorhombic to tetragonal transition that accompanies the transformation of the brownmillerite phase $Ba_2In_2O_5$ to $Ba_2In_2O_5(H_2O)$ [20]. Likewise, in Y-doped $BaCe_{1-x}Y_xO_{3-\delta}$, a more relevant system for PCFC applications, neutron diffraction experiments performed on the $x = 0.20$ solid solution show transitions at 773 K (orthorhombic, *Imma*), 873 K (rhombohedral, $R\bar{3}c$), and 1073 K (cubic, $Pm\bar{3}m$) [21] and the stability of the phases can be correlated with the degree of hydration. Phase transitions are suppressed by the presence of oxygen vacancies and the protonic defects increase the tendency for octahedral tilting, as shown by Andersson et al. [8]. This shifts the stability of lower symmetry phases to higher temperatures and promotes a monoclinic *I2/m* structure at temperature below 673 K. These examples show that the hydration-dehydration behaviour in proton conductors can be complex. Development of methods to investigate systems under conditions that mimic those found in a device is necessary and may also shorten the development cycle of new materials.

Relatively few studies have focussed on the proton conductivity of $BaTiO_3$-based solid solutions, and most concern pristine or 5–10% doped materials [11, 22–26]. The main investigations on heavily doped titanate phases are ionic conduction studies of doped brownmillerite $Ba_2In_2O_5$ [27, 28]. Here, progressively replacing Ti for In induces disordering of the vacancy array, stabilising cubic perovskite structures at room temperature for substitutions larger than 15%. $BaIn_{0.8}Ti_{0.2}O_{3-\delta}$ displays the highest proton conductivity (1.1×10^{-3} S cm^{-1}, under wet N_2 at 723 K), but also a phase transition from cubic $Pm\bar{3}m$ to tetragonal *P4/mmm* upon hydration [29]. Higher doping levels (≥50%) fully stabilise cubic structures, but show poorer protonic conduction [30]. This may be linked to the irregular oxygen sublattice built up by a combination of regular InO_6 and distorted TiO_6 octahedra [31]. A more regular framework for proton mobility is obtained by replacing In^{3+} with the smaller Sc^{3+} (0.80 Å *vs.* 0.74 Å, respectively, when 6-coordinated) that has a strong preference for octahedral environments. The 50% Sc-substituted $BaTiO_3$ [32] is a better proton conductor than its In-doped counterpart [30], under similar conditions. Its proton transference number, t_{H^+}, is close to unitary, below 773 K in a wet inert atmosphere. The 70% Sc-substituted material is able to maintain the same t_{H^+} at higher temperatures [33]. Interestingly, in the $BaTi_{1-x}Sc_xO_{3-\delta}$ system, the Sc doping is structure directing. X-ray diffraction data [33] revealed a phase transformation from a 6H hexagonal perovskite structure for compositions $0.1 \leq x \leq 0.2$, to a cubic perovskite for $0.5 \leq x \leq 0.8$, with an intermediate multiphasic region when $0.3 \leq x \leq 0.5$. In the same study, impedance spectroscopy analyses show how the structural transition impacts on proton mobility, with the highest proton conductivity measured for the cubic $x = 0.7$ (*ca.* 2×10^{-3} S cm^{-1}), whereas in the hexagonal $x = 0.2$ sample performance is reduced by two orders of magnitude, under the same conditions [33]. The behaviour was investigated [34] by means of neutron powder diffraction (NPD) and thermogravimetric analysis (TG), coupled with predictions based on first principle calculations. Ordering of metal dopant, oxygen vacancies and protonic defects was found in the hexagonal $x = 0.2$ type, where protons diffuse *via* higher energy positions. On the contrary, the cubic $x = 0.7$ type is characterised by disorder.

It is clear that Sc levels have a profound effect on the physical properties of these titanate phases and that the cubic members are more interesting from the point of view of the technical applications. Further, a striking point about the 50% Sc-substituted material is that it displays very little chemical expansion of its lattice with the filling of vacancies [32], as per hydration reaction (1). Given the large amount of vacancies that the material can host and that can be filled with protonic defects, this reveals a property that can be crucial for its application as a proton conducting membrane in commercial devices.

This work, hence, explores hydration levels and structural response with a simultaneous thermogravimetric (TG) and *in situ* neutron powder diffraction (NPD) study on two cubic members of the $BaTi_{1-x}Sc_xO_{3-\delta}$ series, with $x = 0.5$ and $x = 0.7$ (BTS50 and BTS70, respectively). With neutrons, crystallographic sites bearing lighter atoms, such as oxygen, can be investigated even in the presence of heavier elements. Therefore, following the evolution of the oxygen site occupancy during dehydration becomes possible, in order to directly link structural parameters and hydration levels to observed mass losses. The structural evolution due to dehydration is discussed in terms of the combination of thermal and chemical expansion in the two systems, and the relative size of vacancies and protonic defects. The aspect of method development is equally important as we hope that demonstrating the feasibility of the experiment will allow further studies on proton conductors and other related materials.

2. Experimental

BTS50 and BTS70 were prepared by solid-state reaction, using carbonate and oxides: $BaCO_3$ (Alfa Aesar, 99.8%), TiO_2 (Sigma-Aldrich, 99.8%), Sc_2O_3 (Alfa Aesar, 99.9%). TiO_2 and Sc_2O_3 were annealed at 1273 K overnight, then stored in a drying oven at 423 K, along with $BaCO_3$, prior to mixing. Stoichiometric mixtures were prepared by manually grinding the reactants in an agate mortar, with ethanol as suspending agent to enhance homogenisation. The finely mixed powders were fired at 1273 K in α-alumina crucibles, then intensively ground and pelletised. The same operations were repeated for every following heating step until phase purity was satisfactory. BTS50 was annealed up to 1773 K, and BTS70 up to 1798 K, with intermediate grinding and pelletising. During the synthesis, sacrificial loose powder was used to cover the faces of the pellets in order to limit volatilisation of BaO, and Ti ions diffusion into the alumina crucible. The samples, placed into α-Al_2O_3 boats, then underwent a hydration step, carried out in a tube furnace through which nitrogen (Air Liquide Alphagaz 1, containing 6 ppm of H_2O) was passed, after bubbling through a round bottom flask filled with distilled water maintained at a constant temperature of 333 K, providing a $p(H_2O)$ of *ca.* 0.2 atm. The samples were exposed to a stepwise temperature programme, from 1073 K to 423 K using the method described in a previous study [34].

Laboratory X-ray powder diffraction data were collected using a Bruker AXS D8 Advance diffractometer equipped with a copper target, a Ge (111) primary monochromator (providing Cu Kα_1 radiation with $\lambda = 1.54056$ Å), and a solid state LynxEye detector. Data were analysed by means of the Rietveld method [35], using the academic version of the software TOPAS v5 [36] (Bruker AXS). The background was modelled with a Chebyshev polynomial function and peak shapes by a convolution of two back-to-back exponentials with a pseudo-Voigt function. For the RT datasets, structural parameters, occupancy factors for the Sc/Ti site, and isotropic displacement parameters were refined. Sequential refinements were performed on cubic lattice parameters, all atomic displacement parameters (ADPs), oxygen site occupancy factors (SOFs), with constrains on Sc/Ti SOFs.

Ex situ thermogravimetric analyses (TGA) were performed on the hydrated samples, in order to determine the degree of saturation of the oxygen vacancies, according to (1). Measurements were carried out on samples of about 60 mg loaded in small α-alumina pans (6 mm diameter), using a Netzsch STA 409 PC Luxx. Temperature programmes were set from room temperature up to 1073 K, at heating rate of 15 K/min, under a flow of 20 ml/min of nitrogen (Air Liquide Alphagaz 1, containing 6 ppm of H_2O).

In situ high-resolution diffraction data were collected on the time-of-flight instrument Polaris at the ISIS neutron and muon source. The samples were loaded into open, cylindrical 8 mm external diameter vanadium cans, then hooked by a fine tungsten wire to the balance of the IGA^n (Intelligent Gravimetric Analyser for neutron experiments, Hiden Isochema) and enclosed in a quartz tube sealed by a Cu gasket. The sample environment was heated up to 573 K by two resistive coils,

one above and one below the sample container, and temperature was monitored by a thermocouple; a similar setup is shown in Wood et al. [6]. The experiments were carried out under vacuum, while pressure was controlled by an inlet and outlet valve through which the system was outgassed at 100 mbar/min. Experiments were started when pressure measured *ca.* 2 mbar, with heating rates set to 0.6 K/min for BTS50 and to 0.5 K/min for BTS70. The choice concerning final temperature and heating rates was determined by the need to accommodate *ca.* 20 h long experiments to the available beam-time. Diffraction data were collected continuously in 10 min blocks, yielding temperature resolution ranging from 6 K at the beginning of the experiments to 2 K towards the end. Rietveld analysis was performed on the data collected on the backscattering bank (0.2–2.65 Å), and 90° bank (up to 4.1 Å).

3. Results

3.1. Pre-characterisation of samples

The X-ray powder diffraction (XPD) data of the hydrated BTS50 and BTS70 were refined according to a cubic perovskite model using space group no. 221, $Pm\bar{3}m$, with structural parameters in agreement with those previously reported by Rahman et al. [32, 33] and Torino et al. [34]. BTS50 was found to be phase pure, while, in BTS70, a low-level parasitic phase, $BaSc_2O_4$, coexisted. This additional phase was refined on the basis of the model proposed by Agafonov et al. [37], giving a refined weight fraction of 3.07(3)%: this was taken into account for all following calculations involving mass changes and stoichiometry. During the syntheses, covering the pellets with sacrificial loose powder proved to be an effective way for preventing Ba and Ti loss, as the diffraction patterns of the loose powders were consistently different from the as-prepared phases.

Sc^{3+} replaces Ti^{4+}, acting as an acceptor dopant, creating oxygen vacancies in order to maintain charge balance within the material (in the Kröger-Vink notation):

$$\mathrm{BaO} + (1\text{–}x)\mathrm{TiO_2} + \frac{x}{2}Sc_2O_3 \rightleftarrows Ba_{Ba}^{x} + (1\text{–}x)\mathrm{Ti}_{Ti}^{x} + \; x\; Sc_{Ti}' + \left(\frac{3\text{–}x}{2}\right)O_O^{x} + \frac{x}{2}\,v_O^{\cdot\cdot} \tag{2}$$

According to (2), and assuming that all scandium is present as Sc^{3+} and titanium as Ti^{4+}, the ideal hydrated compositions, for BTS50 and BTS70 respectively, are $BaSc_{0.5}Ti_{0.5}O_{2.75}(H_2O)_{0.25}$ and $BaSc_{0.7}Ti_{0.3}O_{2.65}(H_2O)_{0.35}$, leading to theoretical mass losses of 1.94% and 2.72%, when all oxygen vacancies are filled with water. The *ex situ* TGA measured mass losses of 1.66% for BTS50 and 2.45% for BTS70, over the range RT-1073 K. The results indicated levels of saturation not corresponding to fully hydrated materials. Rather, under the assumption of ideal compositions, 85.6% for BTS50 and 90.0% for BTS70. Water contents extracted from *ex-situ* TGA data were used to adjust and constrain O and H occupancies in the following refinements. Oxygen site ADPs were refined using an isotropic model in order to reduce the number of free variables. The proton site was modelled according to Torino et al. [34] Fig. 1 and Table 1 summarise the refined NPD room temperature data. The models used for the refinements of RT data yielded the compositions of the hydrated samples: $BaSc_{0.494(4)}Ti_{0.506(4)}O_{2.753}(H_2O)_{0.214}$ for BTS50, and $BaSc_{0.663(5)}Ti_{0.337(5)}O_{2.669}(H_2O)_{0.315}$ for BTS70. This information was used to define the starting models for the sequential refinements. For the latter, the proton site was not included since the poor statistics of fast data-set collection from an evolving system, combined with the background originating from the quartz cell, produced poorer refinements. Several *d*-ranges, with peaks originating from the sample environment, were excluded, as observed by Wood et al. [6].

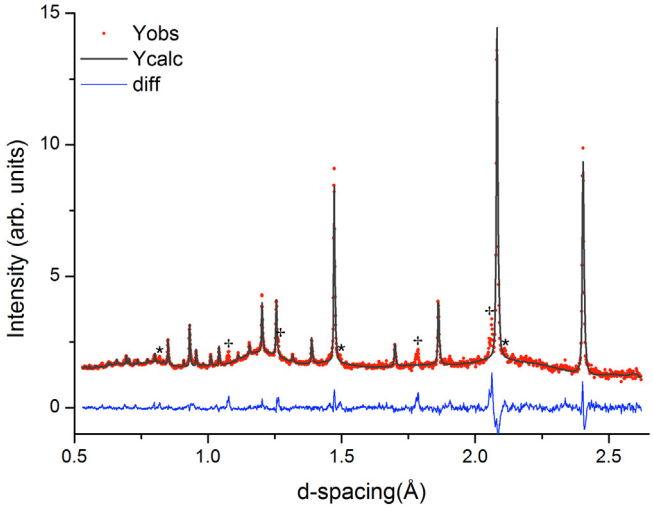

Fig. 1. Refined RT NPD data for hydrated BTS70. The plot shows data collected on the backscattering bank as red dots, the fitted profile as the black solid line, the difference between observed and calculated pattern in blue. Diffraction peaks due to the sample environment are denoted as crosses (+, IGA^n encasement) and asterisks (*, Vanadium can). (For interpretation of the references to colour in this figure legend, the reader is referred to the web version of this article.)

3.2. Simultaneous in situ NPD and TGA

The data collected during the *in situ* thermodiffracto-gravimetric experiment, show a lower dehydration onset temperature for BTS50 (Fig. 2). The derivative of the mass change with respect to temperature was calculated from the raw TG data, and smoothed by averaging the datapoints to obtain resolutions ranging from 10 K around RT, to 2 K around 573 K. Extracted dehydration rates (DR) and cell parameters from refined NPD data reveal peculiarities that are characteristic of the respective Sc-doping level (Fig. 3, *a* and *b*). For BTS50, the thermal evolution of the lattice parameter can be divided into four regions. In the first region, from RT to 413 K, the lattice parameter increases linearly with temperature and a thermal expansion coefficient (TEC) of $4.3 \times 10^{-5}\,K^{-1}$ is calculated. At 413 K, the 0.05% of the initial mass is lost and the temperature onset of dehydration is evident, at a DR of 0.05(1) mg/K, or $2.77(1) \times 10^{-6}\,mol_{H_2O}/K$. Until 493 K, the evolution of the lattice parameter diverges from the previous trend and a region with a steeper slope is observed, with a TEC of $5.9 \times 10^{-5}\,K^{-1}$. Between 493 and 533 K a plateau is observed, where the IGA^n measures 99.18% to 98.56% of the initial mass. At a DR of 0.71(1) mg/K ($3.94(1) \times 10^{-5}\,mol_{H_2O}/K$), the cubic lattice parameter stabilises at around 4.1325(4) Å. The thermal expansion is delayed until the DR drops to 0.30(1) mg/K ($1.66(1) \times 10^{-5}\,mol_{H_2O}/K$). Below this limit the fourth region is observed, where the expansion of the unit cell continues until 573 K, with a TEC of $3.8 \times 10^{-5}\,K^{-1}$. At 573 K the sample is 94.4% dehydrated, 1.57% of the initial mass is lost and the lattice parameter measures 4.1339(4) Å, with a dehydration rate of 0.05(1) mg/K.

The thermal evolution of BTS70's lattice parameter can also be divided into four regions. The expansion of the unit cell between RT and 493 K is linear, with a TEC of $4.5 \times 10^{-5}\,K^{-1}$. Between 493 and 513 K the expansion drastically decelerates under the effect of the increase in DR from 0.53(1) mg/K ($2.94(1) \times 10^{-5}\,mol_{H_2O}/K$) up to 0.78(1) mg/K ($4.33(1) \times 10^{-5}\,mol_{H_2O}/K$). This plateau-like region extends from 99.49% to 99.15% of the sample initial mass, with the lattice parameter stable around 4.1663(4) Å. Above 513 K the unit cell shrinks and we observe the maximum DR of 0.96(1) mg/K ($5.33(1) \times 10^{-5}\,mol_{H_2O}/K$), at 525.5 K, corresponding to 98.90% of the initial mass. Between 513 and 553 K an expansion coefficient of $-4.1 \times 10^{-5}\,K^{-1}$ is calculated.

Table 1
Summary of the results obtained from the Rietveld analysis of NPD data for $BaSc_{0.494(4)}Ti_{0.506(4)}O_{2.753}(H_2O)_{0.214}$ (BTS50), and $BaSc_{0.663(5)}Ti_{0.337(5)}O_{2.669}(H_2O)_{0.315}$ (BTS70), in the cubic crystal system at room temperature (space group: $Pm\bar{3}m$).

	BTS50	BTS70
a (Å)	4.1231(1)	4.1579(2)
Ba 1b (½, ½, ½)		
B_{iso} (Å^2)	0.0161(6)	0.0244(8)
Sc/Ti 1a (0, 0, 0)		
Occ. factor	0.494(4)/0.506(4)	0.663(5)/0.337(5)
B_{iso} (Å^2)	0.0127(7)	0.0232(7)
O 3d (½, 0, 0)		
Occ. factor	0.988	0.995
B_{iso} (Å^2)	0.0117(2)	0.0138(4)
H 24k (x, y, 0)	0.241, 0.399	0.241, 0.399
Occ. factor	0.018	0.026
B_{iso} (Å^2)	0.02	0.02
R_{wp} (%)	3.95	3.40
R_{Bragg} (%)	2.70	2.93

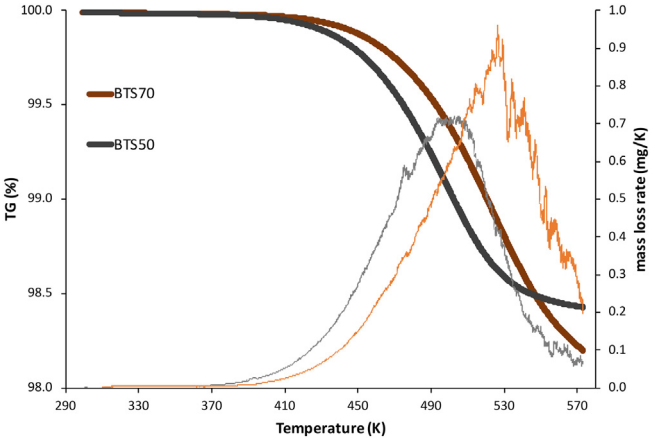

Fig. 2. IGA^n thermograms of BTS50 and BTS70, and relative derivatives in the paler colour shades.

At 553 K, corresponding to 98.40% of the initial mass, the DR is 0.53(1) mg/K and the lattice parameter 4.1648(4) Å. Beyond 553 K the lattice parameter curve starts flattening and the unit cell starts stabilising again, with a lattice constant of 4.1644(4) Å at 573 K. Here, the sample lost 1.8% of its initial mass and it is still about 25% hydrated.

Fig. 4a and b, show the evolution of the oxygen site occupancies with respect to temperature. For both systems, refined oxygen SOFs curves show trends superimposable to TG signals. This allowed us to correlate the dehydration processes to the respective structural responses of BTS50 and BTS70.

4. Discussion

From inspection of the diffractograms, the simple cubic perovskite structural model is retained for both BTS50 and BTS70, at room temperature and above. Constrained refinements of NPD RT data confirmed the hydration level for BTS50 (86.6%), and demonstrated that BTS70 was close to its saturation limit, being 95.2% hydrated. Assuming Sc to be trivalent and Ti as tetravalent, NPD data indicate, in fact, a composition for BTS50, $BaSc_{0.494(4)}Ti_{0.506(4)}O_{2.753}(H_2O)_{0.214}$, that agrees with the expected stoichiometry.

The refined composition for BTS70, $BaSc_{0.663(5)}Ti_{0.337(5)}O_{2.669}(H_2O)_{0.315}$, is below the intended stoichiometry of $BaSc_{0.7}Ti_{0.3}O_{2.65}(H_2O)_{0.35}$ but is consistent with the presence of the secondary phase $BaSc_2O_4$. The different degree of success of the hydration reaction (1) can be explained by the compositional dependence of the hydration thermodynamics for the two systems. For Sc-doped $BaTiO_3$ systems, $\Delta_{Hydr}H^\circ$ becomes less negative with

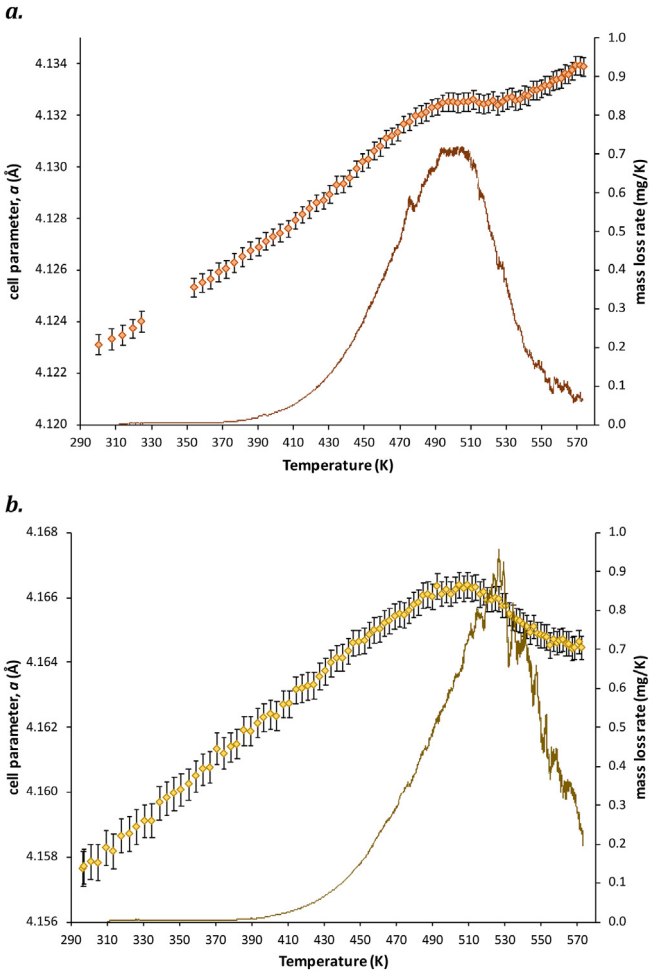

Fig. 3. Evolution of the lattice parameters for BTS50 (*a*), and BTS70 (*b*), plotted against the derivatives of the mass losses. Datapoints are plotted with 3σ significance.

smaller dopant content (−83(2) kJ/mol for BTS70 *vs.* −57(2) kJ/mol for BTS50) [38], decreasing both temperature onset of hydration and temperature of saturation. For BTS50, hence, a longer time is required to reach equilibrium (1) since lower temperatures slow the diffusion of protonic defects.

The data extracted from the IGA^n demonstrate the conclusions Bjørheim et al. [38] drawn from the thermodynamics study of the Sc-

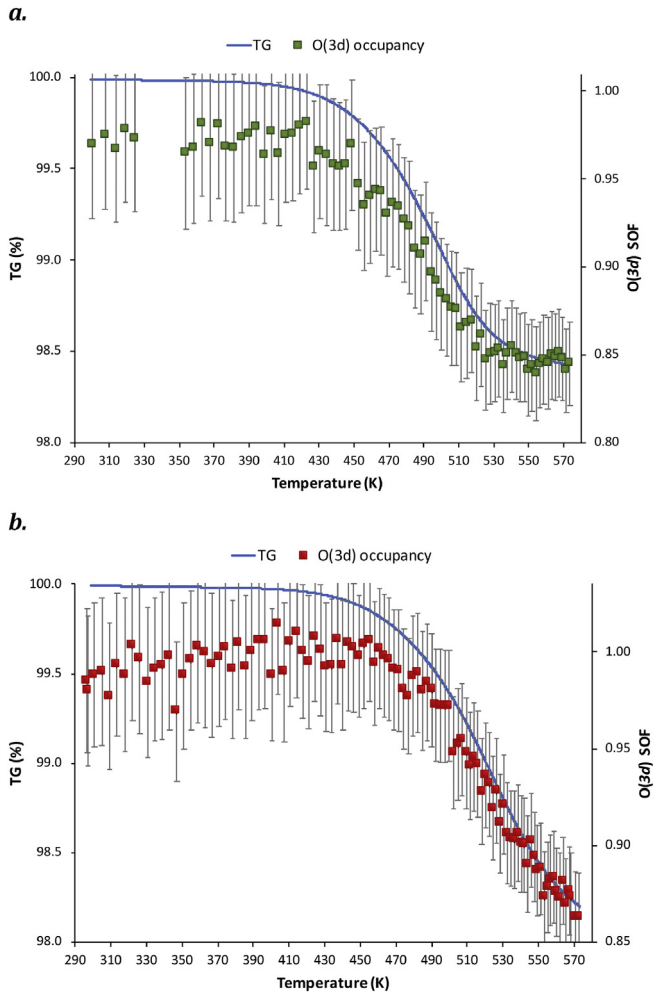

Fig. 4. Evolution of the oxygen site occupancies for BTS50 (*a*), and BTS70 (*b*), plotted against the respective thermograms. Datapoints are plotted with 3σ significance.

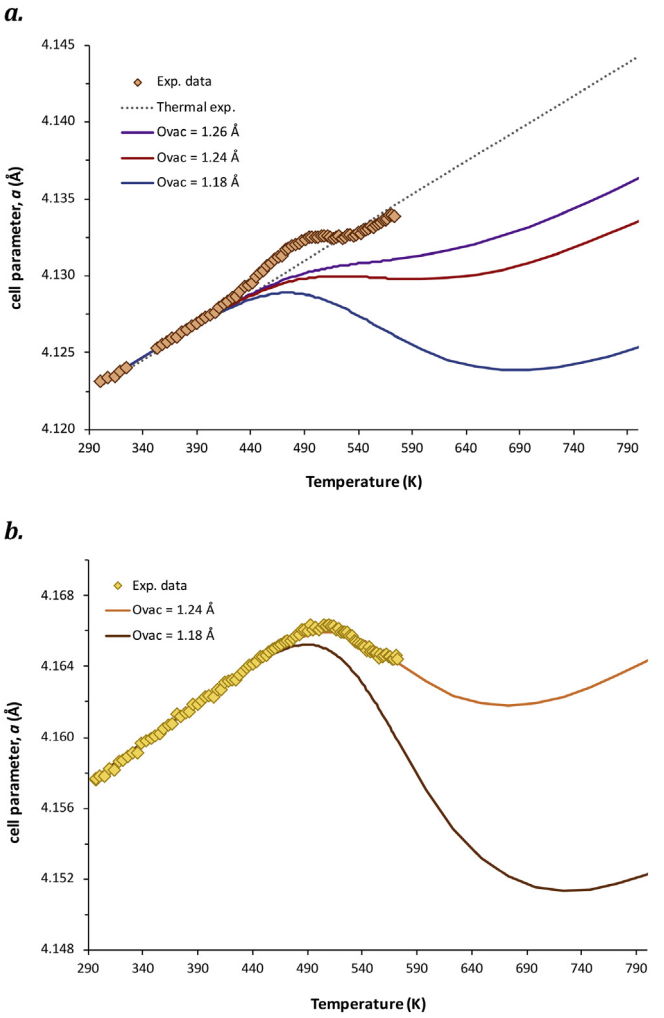

Fig. 5. Evolution of the lattice parameters with temperature, during dehydration, for BTS50 (*a*), and BTS70 (*b*). The dotted line in figure *a.* shows the modelled evolution of the hydrated material solely by thermal expansion. The modelled curves of chemical expansion are shown by the solid lines, with the respective oxygen vacancy size as in the legend.

doped $BaTiO_3$ systems: the enthalpy of proton mobility, $\Delta H_{m,H^+}$, increases with the dopant concentration, 40(5) kJ/mol for BTS50 and 60(5) kJ/mol for BTS70. This indicates that higher temperatures are required for BTS70 to mobilise protons, which is reflected by its higher temperature onset of dehydration, measured at around 423 K (see Fig. 2). Heating rates have an impact on onset temperatures of dehydration, with faster rates shifting the onset towards higher temperatures. Despite the slightly faster heating rate set for BTS50, the expected behaviour was observed on the IGA^n, and confirmed by *ex situ* TG data, where conditions were the same.

In an attempt to gain further insights into the balance between chemical and thermal expansion effects in the two systems, the model reported in Andersson et al. [19] was used to simulate the cell parameter dependence. The results are shown in Fig. 5. The model uses established thermodynamics formalisms to predict the equilibrium concentration of protonic defects and applies this to calculate the perovskite cell parameter based on the summation of the average cation (Ti and Sc) and anion sites ($O_O^\times$, $OH_o^\bullet$ and $v_O^{\bullet\bullet}$) [18]. The ionic radii of Ti^{4+} and Sc^{3+} with 6-fold coordination were used [39], and following Andersson et al. [19], the size of oxygen ion and –OH group were taken as 1.38 Å and 1.35 Å respectively. The effective "size" of the $v_O^{\bullet\bullet}$ is not known and different values were used in the simulations, including 1.18 Å that was used in the original work [19]. The size and shape of the oxygen vacancy has, in fact, been a topic of several studies. Focussing on perovskite-structured oxides, Jedvik et al. [40], employing density functional theory (DFT) calculations on acceptor-doped $BaZrO_3$, proposed an ellipsoidal shape for the oxygen vacancy, with semi-principal axes measuring $r_{vac,x}$ = 1.18 Å, and $r_{vac,y} = r_{vac,z}$ = 0.58 Å. Marrocchelli et al. [41], using both DFT calculations and molecular dynamics simulations, found that r_{vac} ranges from 1.24 Å to 1.57 Å. Noticeably the lattice contracts when an oxygen vacancy is created therefore it is reasonable to imagine a vacancy smaller than an oxide ion. The size of a vacancy seems also to be sensitive to the kind of dopant and its concentration though a clear trend is yet to be found. New experimental data on perovskite systems will eventually help rationalising our current understanding, with the present approach proving to be useful in gathering new information.

The enthalpies of hydration and entropy for these two systems were taken from the values reported in Bjørheim et al. [38] based on DSC measurements, and the partial pressure was adjusted in order to reflect the dehydration temperature displayed by the samples. The simulated cell parameter was then obtained by using the initial TEC and the additional contributions from the chemical expansion. In the model, this component reflects the greater average size of the $OH_o^\bullet$ defects in comparison to the $v_O^{\bullet\bullet}$ that overrides the expected decrease resulting from conversion of a lattice oxygen to an $OH_o^\bullet$ defect. As dehydration occurs at the temperature predicted based on the thermodynamics properties this contribution decreases gradually to zero.

The figure underlines that the chemical expansion (in this case

Table 2
A summary of normalised chemical strain ($\varepsilon_C/\Delta x$) due to hydration of proton conducting ceramic oxides. See text for definition of the terms presented.

Material	ε_C	Δx	$\varepsilon_C/\Delta x$	References	Method
$BaSc_{0.5}Ti_{0.5}O_{3-\delta}$	6.29×10^{-4}	0.3695	1.7×10^{-3}	[32]	XRD
$BaSc_{0.661}Ti_{0.339}O_{2.65}$	3.58×10^{-3}	0.72	4.97×10^{-3}	[34]	NPD
$BaIn_{0.5}Ti_{0.5}O_{3-\delta}$	2.02×10^{-3}	0.285	7.09×10^{-3}	[30]	XRD
$BaZr_{0.5}Yb_{0.5}O_{3-\delta}$	3.32×10^{-3}	0.14	2.37×10^{-2}	[49]	XRD
$BaZr_{0.5}In_{0.5}O_{3-\delta}$	9.53×10^{-3}	0.415	2.3×10^{-2}	[50]	XRD
$BaZr_{0.9}Sc_{0.1}O_{3-\delta}$	7.88×10^{-4}	0.058	1.36×10^{-2}	[51]	XRD[a]
$BaSn_{0.6}Sc_{0.4}O_{3-\delta}$	5.24×10^{-3}	0.4[b]	1.31×10^{-2}	[52]	NPD[a]
$BaCe_{0.8}Y_{0.2}O_{2.9}$	5.2×10^{-3}	0.26	2×10^{-2}	[19]	XRD
$BaZr_{0.9}Y_{0.1}O_{2.95}$	1.5×10^{-3}	0.10	1.5×10^{-2}	[19]	XRD
$BaZr_{0.8}Y_{0.2}O_{2.9}$	3.4×10^{-3}	0.104	3.3×10^{-2}	[19]	XRD

[a] Samples hydrated with D_2O.
[b] Water content assumed to correspond to half the acceptor dopant level.

chemical contraction due to dehydration) of BTS50 is both quite remarkable in nature and very small in magnitude. In particular, the increased rate of cell *expansion* in the T region 450 to 500 K is clear despite the mass loss shown in the simultaneous IGA^n data indicating significant dehydration. This leads to the large divergence between the experimental data and the simulated trend lines that follow the mass loss data more closely. In contrast, for BTS70 the behaviour is more conventional. The overall magnitude of unit cell contraction is simulated with a reasonable accuracy using for $v_O^{\cdot\cdot}$ the value 1.24 Å. Here, the lack of experimental data to higher temperatures results in a limitation in the comparison with the simulated trend.

The overall magnitude of chemical expansion in BTS50 is very small, as judged based on a comparison of the normalised chemical strain determined by comparing cell parameters at RT presented in Table 2.

The *chemical strain*, $\varepsilon_c = (a - a_0) / a_0$, where a represents the lattice parameter of the hydrated material, and a_0 its lattice parameter at a reference chemical composition (in this case when the material is dried), is employed as a measure of the effect of the *chemical expansion*, a concept introduced and formalised by Adler [42] as a new property of electrochemical ceramics. Used as a means to better understanding the relationship between local electronic and defect structure in perovskite-like cobaltite phases as electrode materials for SOFCs [43, 44], the formalism was applied to compare unit cell expansions due to hydration in perovskite-like SOFC electrolyte materials by Andersson et al. [19]. Here, the *normalised chemical strain*, $\varepsilon_c/\Delta x$, relates the chemical strain to the difference in chemical composition (namely the moles of protons/deuterons per formula unit) of the material when hydrated, x, and when dried, x_0.

Table 2 shows that titanate systems display a smaller expansion on hydration, with respect to the well-known cerate and zirconate systems, with BTS50 displaying the smallest expansion. This indicates that the size difference between the $v_O^{\cdot\cdot}$ and the protonic defects is small for this system, and certainly smaller than that for the BTS70 sample. Both systems are very heavily substituted, and support a high level of oxygen deficiency when dry within the framework of a highly disordered perovskite structure. It is therefore reasonable to suspect that short range oxygen vacancy to vacancy correlations exist and this leads to some extent of vacancy clustering, possibly also associated with localised B-site ordering. This, in turn, will influence the cell parameter in the dry state, and consequently also impact the magnitude of the chemical expansion linked to hydration of the vacancies.

A working hypothesis is then that vacancy-vacancy interactions are important in these systems, and that for BTS50 this results in an "average" oxygen vacancy size that is closer to the size of protonic defects than for BTS70. Bearing in mind that hydration both replaces a vacancy with a protonic defect, and converts an oxide ion to a smaller –OH group, the net chemical expansion will consequently be much smaller in BTS50. Further studies are required to investigate the degree of short range correlations within these systems in both dry and hydrated forms. The use of neutron diffraction data and the total scattering approach, as applied recently to ordering effects in fluorites/pyrochlores [45, 46] is planned in the near future and may provide further information regarding the chemical strain effects. Regardless of the exact mechanism at play it is clear that the applicability of the simple point defect model used to simulate the cell parameter is more questionable for these heavily substituted samples in comparison to the lower substitution levels of $BaZr_{1-x}Y_xO_{3-x/2}$ ($0.05 \le x \le 0.20$) and $BaCe_{0.8}Y_{0.2}O_{3-\delta}$ perovskites it was first applied to [19].

A stronger vacancy-vacancy interaction might also explain why the enthalpy of vacancy mobility, $\Delta H_{m,v_O^{\cdot\cdot}}$, diminishes at higher Sc concentrations (95(5) kJ/mol for BTS50 and 66(5) kJ/mol for BTS70) [38]. The interaction between vacancies could make it necessary to supply more energy to mobilise a vacancy due to clustering, implying a stabilisation of oxygen vacancies at higher temperatures for the lower substitution levels. On the other hand, the relative stability of vacancies and protonic defects may vary with the hydration level. ^{45}Sc NMR studies [47] and DFT calculations [48] performed on 10 mol% Sc-doped $BaZrO_3$, show how fully hydrated samples tend to disfavour proton migration because of the attractive nature of the Coulombic interaction between the positively charged protonic defect and the negatively charged acceptor dopant site. As the concentration of protonic defects diminishes, the association of dopant and oxygen vacancies, which start to form around the acceptor dopant site, produces a positive net charge that repels the protonic defects and may disrupt the anisotropic distribution of protons creating local ordering effects. As noted by the authors of these studies, oxygen vacancies are very stable when in a Sc'_{Zr}—$v_O^{\cdot\cdot}$—Sc'_{Zr} associated complex configuration and it may be argued that this stability produces the differences in the measured $\Delta H_{m,v_O^{\cdot\cdot}}$. However, given the different environment in which vacancies are found, comparing data between zirconate and titanate systems can be difficult, especially differences in dopant concentration, and the combination of a total scattering method with the previous observations on Sc-doped and substituted systems will provide further insight.

A possible explanation for the unexpected increase in cell expansion during dehydration is that the thermal expansion coefficient of BTS50 increases as it dehydrates, and that this counteracts the cell contraction resulting from the loss of protonic defects. As noted above, as the size difference between these two species appears to be particularly small for this system, the material can effectively reach a point where $[OH_o^{\cdot}] \approx [v_O^{\cdot\cdot}]$ before the chemical contraction can balance this increased rate of thermal expansion leading to a small plateau region where the cell parameter is constant as temperature increases. Further studies are required to understand the effect of hydration level on TEC.

5. Conclusion

Hydration-dehydration cycles are critical to proton conductors and neutrons are ideal to probe oxygen sites in the presence of heavier elements. The simultaneous *in situ* NPD and TG analysis of our systems

allowed us to correlate dehydration properties to structural responses, in a way *ex situ* and independent studies cannot. It is, in fact, often difficult to connect *ex situ* data from different techniques with great confidence since conditions experienced by the samples are usually not exactly the same. This study was successful in directly linking oxygen occupancy, and therefore water content, to gravimetric data. This link was instrumental in correlating lattice changes to dehydration rates, information that is vital for understanding the complex chemical expansion strain effects and, in the future, for lattice matching multi-component devices. Finally, *ex situ* thermodynamics data from previous studies were rationalised with the direct observation of their effect on evolving systems during the thermally induced dehydration.

In BTS50, the size difference between the protonic defects and the oxygen vacancy is suggested to be anomalously small and the rate of thermal expansion appears to be influenced by the level of hydration. These two effects mean that thermal expansion compensates the contraction caused by dehydration and associated vacancy formation, ultimately leading to a plateau region for the unit cell parameter. In BTS70, the observed cell dependence is more conventional in nature, with the cell contraction observed during de-hydration indicating the chemical expansion contribution is larger for the more heavily scandium substituted system. Further studies aiming to clarify the local structural dependence of these highly oxygen deficient systems in both hydrated and dry states are planned.

Acknowledgements

The authors acknowledge the Interreg Programme for funding the project (grant number CTH-001). We would also like to thank the ISIS neutron and muon facility for access to scheduled beam-time (RB 1510335, DOI: https://doi.org/10.5286/ISIS.E.73947824). Special thanks go to Dariusz Wardecki for his assistance with the software TOPAS v5.

References

[1] F. Mauvy, P. Berger, N. Sata, P.R. Slater, Characterization tools, in: M. Marrony (Ed.), Proton-conducting Ceramics, Taylor & Francis Group, LLC, 2016, pp. 17–62 (ISBN: 978-981-4613-85-9).
[2] M.A. Tamimi, S. Mcintosh, High temperature in situ neutron powder diffraction of oxides, J. Mater. Chem. A 2 (2014) 6015–6026, https://doi.org/10.1039/c3ta14159d.
[3] M. Gaboardi, S. Duyker, C. Milanese, G. Magnani, V.K. Peterson, D. Pontiroli, et al., In situ neutron powder diffraction of Li_6C_{60} for hydrogen storage, J. Phys. Chem. C 119 (2015) 19715–19721, https://doi.org/10.1021/acs.jpcc.5b06711.
[4] D. Goonetilleke, J.C. Pramudita, M. Hagan, O.K. Al Bahri, W.K. Pang, V.K. Peterson, et al., Correlating cycling history with structural evolution in commercial 26650 batteries using in operando neutron powder diffraction, J. Power Sources 343 (2017) 446–457, https://doi.org/10.1016/j.jpowsour.2016.12.103.
[5] S.T. Norberg, G. Azimi, S. Hull, H. Leion, In situ neutron powder diffraction study of the reaction $M_2O_3 \longleftrightarrow M_3O_4 \longleftrightarrow MO$, M = $(Fe_{0.2}Mn_{0.8})$: implications for chemical looping combustion, CrystEngComm 18 (2016) 5537–5546, https://doi.org/10.1039/C6CE00784H.
[6] T.J. Wood, J.W. Makepeace, W.I.F. David, Neutron diffraction and gravimetric study of the iron nitriding reaction under ammonia decomposition conditions, Phys. Chem. Chem. Phys. 19 (2017) 27859–27865, https://doi.org/10.1039/C7CP04494A.
[7] F.G. Kinyanjui, S.T. Norberg, I. Ahmed, S.G. Eriksson, S. Hull, In-situ conductivity and hydration studies of proton conductors using neutron powder diffraction, Solid State Ionics 225 (2012) 312–316, https://doi.org/10.1016/j.ssi.2012.05.018.
[8] A.K. Eriksson Andersson, S.M. Selbach, T. Grande, C.S. Knee, Thermal evolution of the crystal structure of proton conducting $BaCe_{0.8}Y_{0.2}O_{3-\delta}$ from high-resolution neutron diffraction in dry and humid atmosphere, Dalton Trans. 44 (2015) 10834–10846, https://doi.org/10.1039/c4dt03948c.
[9] K. Bae, D.Y. Jang, H.J. Choi, D. Kim, J. Hong, B. Kim, et al., Demonstrating the potential of yttrium-doped barium zirconate electrolyte for high-performance fuel cells, Nat. Commun. 8 (2017) 1–9, https://doi.org/10.1038/ncomms14553.
[10] Y. Yamazaki, R. Hernandez-sanchez, S.M. Haile, High total proton conductivity in large-grained yttrium-doped barium zirconate, Chem. Mater. 51 (2009) 2755–2762, https://doi.org/10.1021/cm900208w.
[11] K.D. Kreuer, Aspects of the formation and mobility of protonic charge carriers and the stability of perovskite-type oxides, Solid State Ionics 125 (1999) 285–302, https://doi.org/10.1016/S0167-2738(99)00188-5.
[12] T. Schober, H.G. Bohn, Water vapor solubility and electrochemical characterization of the high temperature proton conductor $BaZr_{0.9}Y_{0.1}O_{2.95}$, Solid State Ionics 127 (2000) 351–360, https://doi.org/10.1016/S0167-2738(99)00283-0.
[13] D. Han, N. Hatada, T. Uda, Chemical expansion of yttrium-doped barium zirconate and correlation with proton concentration and conductivity, J. Am. Ceram. Soc. 99 (2016) 3745–3753, https://doi.org/10.1111/jace.14377.
[14] C. Duan, J. Tong, M. Shang, S. Nikodemski, M. Sanders, S. Ricote, et al., Readily processed protonic ceramic fuel cells with high performance at low temperatures, Science 349 (2015) 1321–1326 (80), https://doi.org/10.1126/science.aab3987.
[15] D. Pergolesi, E. Fabbri, A.D. Epifanio, E. Di Bartolomeo, A. Tebano, S. Sanna, et al., High proton conduction in grain-boundary-free yttrium-doped barium zirconate films grown by pulsed laser deposition, Nat. Mater. 9 (2010) 846–852, https://doi.org/10.1038/nmat2837.
[16] S. Nikodemski, J. Tong, R. O'Hayre, Solid-state reactive sintering mechanism for proton conducting ceramics, Solid State Ionics 253 (2013) 201–210, https://doi.org/10.1016/j.ssi.2013.09.025.
[17] M. Hakim, C. Yoo, J.H. Joo, J.H. Yu, Enhanced durability of a proton conducting oxide fuel cell with a purified yttrium-doped barium zirconate-cerate electrolyte, J. Power Sources 278 (2015) 320–324, https://doi.org/10.1016/j.jpowsour.2014.12.046.
[18] K.D. Kreuer, Proton-conducting oxides, Annu. Rev. Mater. Res. 33 (2003) 333–359, https://doi.org/10.1146/annurev.matsci.33.022802.091825.
[19] A.K.E. Andersson, S.M. Selbach, C.S. Knee, T. Grande, Chemical expansion due to hydration of proton-conducting perovskite oxide ceramics, J. Am. Ceram. Soc. 97 (2014) 2654–2661, https://doi.org/10.1111/jace.12990.
[20] T. Schober, J. Friedrich, F. Krug, Phase transition in the oxygen and proton conductor $Ba_2In_2O_5$ in humid atmospheres below 300 °C, Solid State Ionics 99 (1997) 9–13, https://doi.org/10.1016/S0167-2738(97)00203-8.
[21] L. Malavasi, C. Ritter, G. Chiodelli, Correlation between thermal properties, electrical conductivity, and crystal structure in the $BaCe_{0.80}Y_{0.20}O_{2.9}$ proton conductor, Chem. Mater. 20 (2008) 2343–2351, https://doi.org/10.1021/cm7033917.
[22] J.M. Pope, The use of $BaTiO_3$ as a solid-electrolyte to determine water vapor effects upon electrical transport mechanisms, Mater. Res. Bull. 9 (1974) 1111–1118, https://doi.org/10.1016/0025-5408(74)90026-9.
[23] W. Münch, K.D. Kreuer, G. Seifert, J. Maier, Proton diffusion in perovskites: comparison between $BaCeO_3$, $BaZrO_3$, $SrTiO_3$, and $CaTiO_3$ using quantum molecular dynamics, Solid State Ionics 136–137 (2000) 183–189, https://doi.org/10.1016/S0167-2738(00)00304-0.
[24] K.D. Kreuer, S. Adams, W. Münch, A. Fuchs, U. Klock, J. Maier, Proton conducting alkaline earth zirconates and titanates for high drain electrochemical applications, Solid State Ionics 145 (2001) 295–306, https://doi.org/10.1016/S0167-2738(01)00953-5.
[25] T. Schober, A. Magrez, Sol-gel preparation of selected high temperature proton conductors, Kiel 10 (2004) 17–19, https://doi.org/10.1007/BF02410299.
[26] H. Jena, K.V. Govindan Kutty, T.R.N. Kutty, Proton transport and structural relations in hydroxyl-bearing $BaTiO_3$ and its doped compositions synthesised by wet-chemical methods, Mater. Res. Bull. 39 (2004) 489–511, https://doi.org/10.1016/j.materresbull.2003.10.004.
[27] V. Jayaraman, A. Magrez, M. Caldes, O. Joubert, M. Ganne, Y. Piffard, et al., Characterization of perovskite systems derived from $Ba_2In_2O_5\square$ – part I: the oxygen-deficient $Ba_2In_{2(1-x)}Ti_{2x}O_{5+x}\square_{1-x}$ ($0 \le x \le 1$) compounds, Solid State Ionics 170 (2004) 17–24, https://doi.org/10.1016/S0167-2738(03)00300-X.
[28] V. Jayaraman, A. Magrez, M. Caldes, O. Joubert, F. Taulelle, J. Rodriguez-Carvajal, et al., Characterization of perovskite systems derived from $Ba_2In_2O_5\square$ – part II: the proton compounds $Ba_2In_{2(1-x)}Ti_{2x}O_{4+2x}(OH)_y$ [$0 \le x \le 1$; $y \le 2(1-x)$], Solid State Ionics 170 (2004) 25–32, https://doi.org/10.1016/S0167-2738(03)00299-6.
[29] E. Quarez, S. Noirault, M.T. Caldes, O. Joubert, Water incorporation and proton conductivity in titanium substituted barium indate, J. Power Sources 195 (2010) 1136–1141, https://doi.org/10.1016/j.jpowsour.2009.08.086.
[30] S.M.H. Rahman, C.S. Knee, I. Ahmed, S.G. Eriksson, R. Haugsrud, 50 Mol% indium substituted $BaTiO_3$: characterization of structure and conductivity, Int. J. Hydrog. Energy 37 (2012) 7975–7982, https://doi.org/10.1016/j.ijhydene.2011.12.139.
[31] S.T. Norberg, S.M.H. Rahman, S. Hull, C.S. Knee, S.G. Eriksson, The proton conducting electrolyte $BaTi_{0.5}In_{0.5}O_{2.75}$: determination of the deuteron site and its local environment, J. Phys. Condens. Matter 25 (2013) 454214, , https://doi.org/10.1088/0953-8984/25/45/454214.
[32] S.M.H. Rahman, I. Ahmed, R. Haugsrud, S.G. Eriksson, C.S. Knee, Characterisation of structure and conductivity of $BaTi_{0.5}Sc_{0.5}O_{3-\delta}$, Solid State Ionics 255 (2014) 140–146, https://doi.org/10.1016/j.ssi.2013.12.010.
[33] S.M.H. Rahman, S.T. Norberg, C.S. Knee, J.J. Biendicho, S. Hull, S.G. Eriksson, Proton conductivity of hexagonal and cubic $BaTi_{1-x}Sc_xO_{3-\delta}$ ($0.1 \le x \le 0.8$), Dalton Trans. 43 (2014) 15055–15064, https://doi.org/10.1039/c4dt01280a.
[34] N. Torino, P.F. Henry, C.S. Knee, T.S. Bjørheim, S.M.H. Rahman, E. Suard, et al., The influence of cation ordering, oxygen vacancy distribution and proton siting on observed properties in ceramic electrolytes: the case of scandium substituted barium titanate, Dalton Trans. 46 (2017) 8387–8398, https://doi.org/10.1039/c7dt01559c.
[35] H.M. Rietveld, A profile refinement method for nuclear and magnetic structures, J. Appl. Crystallogr. 2 (1969) 65–71, https://doi.org/10.1107/S0021889869006558.
[36] A. Coelho, Topas Academic Version 5, Topas Academic, Coelho Software, Brisbane, 2012.
[37] V. Agafonov, A. Kahn, D. Michel, Crystal structure of $BaSc_2O_4$; its relation with perovskite, Mater. Res. Bull. 18 (1983) 975–981, https://doi.org/10.1016/0025-5408(83)90009-0.
[38] T.S. Bjørheim, S.M.H. Rahman, S.G. Eriksson, C.S. Knee, R. Haugsrud, Hydration thermodynamics of the proton conducting oxygen-deficient perovskite series $BaTi_{1-x}M_xO_{3-x/2}$ with M = In or Sc, Inorg. Chem. 54 (2015) 2858–2865, https://doi.org/10.1021/ic503006u.

[39] R.D. Shannon, Revised effective ionic radii and systematic studies of interatomic distances in halides and chalcogenides, Acta Crystallogr. A32 (1976) 751–767, https://doi.org/10.1107/S0567739476001551.
[40] E. Jedvik, A. Lindman, M.Þ. Benediktsson, G. Wahnström, Size and shape of oxygen vacancies and protons in acceptor-doped barium zirconate, Solid State Ionics 275 (2015) 2–8, https://doi.org/10.1016/j.ssi.2015.02.017.
[41] D. Marrocchelli, N.H. Perry, S.R. Bishop, Understanding chemical expansion in perovskite-structured oxides, Phys. Chem. Chem. Phys. 17 (2015) 10028–10039, https://doi.org/10.1039/C4CP05885B.
[42] S.B. Adler, Chemical expansivity of electrochemical ceramics, J. Am. Ceram. Soc. 19 (2001) 2117–2119.
[43] X. Chen, J. Yu, S.B. Adler, Thermal and chemical expansion of Sr-doped lanthanum cobalt oxide ($La_{1-x}Sr_xCoO_{3-\delta}$), Chem. Mater. 17 (2005) 4537–4546, https://doi.org/10.1021/cm050905h.
[44] H.L. Lein, K. Wiik, T. Grande, Thermal and chemical expansion of mixed conducting $La_{0.1}Sr_{0.9}Co_{0.8}Fe_{0.2}O_{3-\delta}$, Solid State Ionics 177 (2006) 1795–1798, https://doi.org/10.1016/j.ssi.2006.02.033.
[45] S.T. Norberg, S. Hull, S.G. Eriksson, I. Ahmed, F. Kinyanjui, J.J. Biendicho, Pyrochlore to fluorite transition: the $Y_2(Ti_{1-x}Zr_x)_2O_7$ ($0.0 \leq x \leq 1.0$) system, Chem. Mater. 24 (2012) 4294–4300, https://doi.org/10.1021/cm301649d.
[46] L.-E. Kalland, S.T. Norberg, J. Kyrklund, S. Hull, S.G. Eriksson, T. Norby, et al., C-type related order in the defective fluorites $La_2Ce_2O_7$ and $Nd_2Ce_2O_7$ studied by neutron scattering and ab initio MD simulations, Phys. Chem. Chem. Phys. 18 (2016) 24070–24080, https://doi.org/10.1039/C6CP04708D.
[47] I. Oikawa, H. Takamura, Correlation among oxygen vacancies, protonic defects, and the acceptor dopant in Sc-doped $BaZrO_3$ studied by ^{45}Sc nuclear magnetic resonance, Chem. Mater. 27 (2015) 6660–6667, https://doi.org/10.1021/acs.chemmater.5b02441.
[48] H. Takahashi, I. Oikawa, H. Takamura, Atomistic insight into the correlation among oxygen vacancies, protonic defects, and the acceptor dopants in Sc-doped $BaZrO_3$ using first-principles calculations, J. Phys. Chem. C 122 (2018) 6501–6507, https://doi.org/10.1021/acs.jpcc.7b11742.
[49] I. Ahmed, C.S. Knee, S.-G. Eriksson, E. Ahlberg, M. Karlsson, A. Matic, et al., Proton conduction in perovskite oxide $BaZr_{0.5}Yb_{0.5}O_{3-\delta}$ prepared by wet chemical synthesis route, J. Electrochem. Soc. 155 (2008) P97–P102, https://doi.org/10.1149/1.2969806.
[50] I. Ahmed, S.G. Eriksson, E. Ahlberg, C.S. Knee, Influence of microstructure on electrical properties in $BaZr_{0.5}In_{0.5}O_{3-\delta}$ proton conductor, Solid State Ionics 179 (2008) 1155–1160, https://doi.org/10.1016/j.ssi.2008.02.031.
[51] I. Ahmed, M. Karlsson, S.-G. Eriksson, E. Ahlberg, C.S. Knee, K. Larsson, et al., Crystal structure and proton conductivity of $BaZr_{0.9}Sc_{0.1}O_{3-\delta}$, J. Am. Ceram. Soc. 91 (2008) 3039–3044, https://doi.org/10.1111/j.1551-2916.2008.02547.x.
[52] F.G. Kinyanjui, S.T. Norberg, C.S. Knee, I. Ahmed, S. Hull, L. Buannic, et al., Crystal structure and proton conductivity of $BaSn_{0.6}Sc_{0.4}O_{3-\delta}$: insights from neutron powder diffraction and solid-state NMR spectroscopy, J. Mater. Chem. A 4 (2016) 5088–5101, https://doi.org/10.1039/C5TA09744D.